Composites Part B 243 (2022) 110160

Contents lists available at ScienceDirect

Composites Part B

journal homepage: www.elsevier.com/locate/compositesb

Impact of micromechanics on dynamic compressive behavior of ultra-high performance concrete containing limestone powder

Weitan Zhuang [a], Shaohua Li [a], Zhengzhi Wang [a], Zuhua Zhang [c], Qingliang Yu [a,b,*]

[a] School of Civil Engineering, Wuhan University, 430072, Wuhan, PR China
[b] Department of the Built Environment, Eindhoven University of Technology, P.O. Box 513, 5600 MB, Eindhoven, the Netherlands
[c] Key Laboratory for Green & Advanced Civil Engineering Materials and Application Technology of Hunan Province, College of Civil Engineering, Hunan University, 410082, Changsha, PR China

ARTICLE INFO

Keywords:
Ultra-high performance concrete
Limestone powder
Nanoindentation
C–S–H
Strain rate
Energy absorption

ABSTRACT

To improve sustainability and reduce costs, interest in using limestone powder (LP) in ultra-high performance concrete (UHPC) has been increasing in recent years. Incorporating LP changes packing, characteristics of C–S–H and pore structure of interfacial transition zone (ITZ) and matrix by physical and chemical effects. However, the influences of LP replacement on the mechanical properties of UHPC, from micromechanics to macroscopic impact behaviors, have not been well understood. Herein, mercury intrusion porosimetry (MIP), thermal gravimetric (TG), nanoindentation test and Split Hopkinson pressure bar (SHPB) test are performed to reveal the relationships between the micromechanical properties and the dynamic performances of UHPC. Results show that appropriate amount of LP incorporation optimizes the packing, leading to a narrower space and more densely compacted C–S–H that improves the percentages of high-density C–S–H and ultra-high density C–S–H in ITZ. The higher density of C–S–H results in a higher steel fiber-matrix bond strength, which benefits a higher dynamic compressive strength and energy absorption while a lower dynamic increase factor. More low-density C–S–H are generated due to the dilution effect of excessive LP, leading to a weak steel fiber-matrix bond strength that deteriorates the impact resistance. Additionally, the mechanism of LP enhancing the quality of C–S–H in ITZ is proposed, which favors understanding the relation between macro dynamic performance and interfacial behavior at the micro and nanoscale.

1. Introduction

Ultra-high-performance concrete (UHPC) is considered as a relatively innovative and promising building material with excellent mechanical properties, outstanding durability, and superior impact resistance [1–5]. However, UHPC is also featured by extremely low water content and high cement content. Using massive amounts of cement, usually over 900 kg/m^3, results in increased costs, higher energy consumption, and intensive CO_2 emissions [6,7]. The very low water-to-cement ratio (w/c, usually lower than 0.22) leads to a large amount of unhydrated cement in the binder system, which just acts as expensive fillers [8,9]. Hence, replacing cement appropriately with more sustainable supplementary cementitious materials (SCMs) is possible to reduce the costs as well as environmental impact without compromising its performance. Many kinds of SCMs have been introduced into UHPC system. However, some of them, e.g. ground granulated blast slag and fly ash, may not be easily locally available [10]. Instead, owing to the cheap price compared with cement, ease of quality control, homogeneous composition, and worldwide availability, limestone powder (LP) has attracted increasing interest for sustainable development [11–13].

LP has been widely utilized as SCM to accelerate cement hydration and enhance fresh properties of concretes [14]. Owing to the nucleation effect, LP accelerates the hydration of cement by offering extra surfaces for the nucleation and development of the hydration products [15,16]. LP also acts as an active participant in the hydration reactions. It was found that production of monocarbonate in the presence of LP indirectly stabilized ettringite resulting in a corresponding rise in the total volume of the hydrate phase and a decline in porosity, thereby improving the micromechanical properties [17]. Furthermore, LP could react with the alumina phases and produce carboaluminates, which reduces porosity and increases compressive strength [18]. Li et al. [9] found that an

* Corresponding author. School of Civil Engineering, Wuhan University, 430072, Wuhan, PR China.
E-mail address: q.yu@bwk.tue.nl (Q. Yu).

https://doi.org/10.1016/j.compositesb.2022.110160
Received 18 April 2022; Received in revised form 20 June 2022; Accepted 22 July 2022
Available online 1 August 2022

appropriate amount of LP leads to denser pore structure, higher strength, and diminished total free shrinkage. As illustrated above, introducing proper contents of LP into UHPC system could achieve a satisfactory mechanical performance.

Besides the quasi-static loading, UHPC structures, e.g. piers, long-span bridges and protective structures, are susceptible to high strain loading such as weight drop, vehicular loads and blast during the service life [19,20]. The dynamic compression characteristics of UHPC are primarily determined by the quality of the matrix, the steel fiber (characteristics and content), and the bonding force between them [21,22]. The incorporation of steel fibers significantly enhances the toughness and impact resistance of UHPC [23]. The addition of LP would influence the quality of the steel fiber-matrix bond and the matrix of UHPC. Deeper understanding the effect of LP on steel fiber-matrix bond strength would be beneficial for developing UHPC with higher strength and energy absorption under impact loading. Considering the filler effect and hydration capability of LP, the incorporation of LP would lead to different constituent phases of gel, microscopic pore structure at interfacial transition zone (ITZ) and matrix at the micro and nanoscale, which is expected to affect dynamic properties of UHPC. Nonetheless, most of previous researches concerning the influence of LP in UHPC mainly concentrated on the hydration progress, rheological behavior, microstructures, quasi-static mechanical characteristics and durability [24–26], few of them are related to the bond of steel fiber-matrix interface, dynamic properties and the involved relationships. From micro-scale to macro-scale, the influence mechanism of the matrix and bond of steel fiber-matrix induced by LP dosage on the dynamic compression behavior of UHPC is still not clear.

Nanoindentation technique has been proved to be an effective tool to quantitatively explore the micromechanical property of newly developed cementitious composite materials [27–29]. The majority of the previous researches are concentrated on the paste or the aggregate interface in concrete, in which the distribution of the hardness, elastic modulus, fracture toughness and creep behaviors are investigated [30–32]. The addition of LP would influence the types and content of the hydration products, which can be characterized by nanoindentation technique. The changes of hydration products further influence the micromechanical property of steel fiber-matrix interfacial transition zone. The micromechanical property of ITZ is considered as an essential factor affecting the macroscopic performances of UHPC [30]. Therefore, understanding the influential mechanism of LP on the micromechanical properties of ITZ by nanoindentation, further to clarify the bond of fiber-matrix interface, is essential for better understanding the dynamic properties of UHPC. Nevertheless, up to now, limited research has attempted to investigate the effect of the micromechanical property of steel fiber-matrix interfacial transition zone on the dynamic compressive characteristics in UHPC.

This study aims to systematically study the effect of LP replacement on the micromechanical characteristics and its effect on the dynamic compressive performance from a multiscale view. Two steel fiber volume fractions (1% and 2%) and five LP fractions by mass of total powders (10%, 20%, 30%, 40% and 50%) are used. The flowability, pore structure, hydration productions, phase distribution of ITZ, compressive strengths, tensile performance and dynamic compressive properties are tested and analyzed. The dynamic compressive behaviors of UHPC are measured utilizing a 50 mm split Hopkinson pressure bar (SHPB) device. Moreover, the nanoindentation technique is utilized to examine the micromechanical property of steel fiber-matrix interfacial transition zone. Experimental results are expected to promote the understanding of the relationship between macro dynamic performance of UHPC with different LP content and interfacial behavior at the microscale.

2. Experimental program

2.1. Raw materials

The raw materials used in this study are cement PII · 52.5 (PC), limestone powder (LP), micro-silica (mS), polycarboxylate-based superplasticizer (SP) with 30% solid content. The PC consists approximately 4% LP (data provided by the manufacturer and verified by own thermal analysis). Fig. 1 shows the particle size distribution of the materials. The chemical compositions and specific surfaces area of the powders are shown in Table 1. The morphologies of the materials are measured by scanning electron microscopy (SEM), as presented in Fig. 2.

2.2. Mix proportion

In this study, six UHPC paste mixtures are produced with a water-powder ratio (w/p) of 0.18. The six UHPC paste mixtures incorporating 0, 10%, 20%, 30%, 40%, and 50% LP are designated as LP0, LP10, LP20, LP30, LP40, and LP50, respectively. The content of mS is 5% of the whole powder mass, considering both sustainability and performance [33]. Table 2 presents the recipes of UHPC paste. SP refers to the amount of polycarboxylate-based superplasticizer by mass of powders. The dosage of SP is adjusted to achieve self-consolidating properties and ensure the uniform distribution of steel fibers, which will be discussed in detail in Section 3.1. Straight steel fibers with 0.2 mm in diameter and 13 mm in length are utilized. Two steel fiber volume fractions (1% and 2%) are used to investigate the influence of steel fibers on the mechanical performance. The elastic modulus and tensile strength of steel fiber are 200 GPa and 2.25 GPa, respectively. The reinforced UHPC paste with 1% and 2% steel fibers are denoted as LP0-1 and LP0-2, LP10-1 and LP10-2, LP20-1 and LP20-2, LP30-1 and LP30-2, LP40-1 and LP40-2, LP50-1 and LP50-2, respectively.

2.3. Mixing procedure and sample preparation

The detail mixing procedure is as follow: drying mixing all the powders for 1 min, then, adding 75% water and mixing for 1.5 min, remaining water incorporated with SP is added mixing for 2.5 min sequentially, steel fibers are lastly added mixing for about another 5 min. Samples are cast and demolded (cube with the size of 70.7 × 70.7× 70.7 mm^3 for quasi-static compressive strength) after 24 h and then cured in the conditions of 20 ± 2 °C and relative humidity greater than 95%. The specimen used for the dynamic test is made into 50 mm

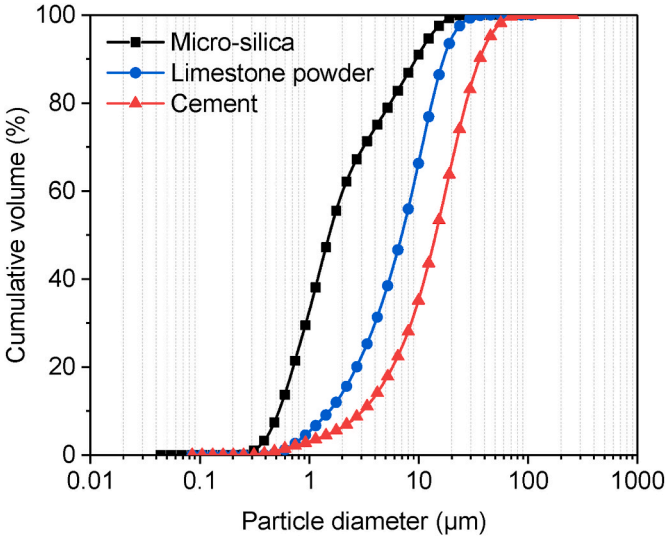

Fig. 1. Particle size distribution of powders.

Table 1
Chemical and physical properties of powders.

Components (%)	PC	mS	LP
CaO	64.61	0.05	53.55
SiO_2	19.2	96.33	0.62
Al_2O_3	4.17	0.16	—
Fe_2O_3	3.69	0.28	0.01
K_2O	0.75	—	0.19
Na_2O	0.19	—	0.64
SO_3	3.33	—	1.88
MgO	1.31	—	0.66
TiO_2	0.22	—	—
MnO	0.10	—	0.01
LOI	2.04	0.88	42.63
Specific density(g/cm^3)	2.99	2.23	2.75
BET surface area (m^2/kg)	944	9716	1353

(diameter) and 25 mm (height), with an aspect ratio of 0.50, which is beneficial to minimize the frictional and inertial effects [5,34]. The specimens are produced following coring, slicing and polishing. Both surfaces of specimens are machined to a roughness of less than 0.02 mm to keep the reliability of the experimental results.

2.4. Experimental program

2.4.1. Flowability

The flowability of UHPC paste is performed by a truncated mold (top diameter: 70 mm, bottom diameter: 100 mm, height: 60 mm), in accordance with EN 1015-3: 2007 [35]. The fluidity of 270 ± 20 mm is achieved by adjusting the SP dosage for the self-consolidating mix.

2.4.2. Thermal gravimetry

To investigate the influence of LP on the hydration products, the thermal gravimetric (TG) and the differential thermal gravimetric (DTG) analysis are conducted by a Netzsch simultaneous analyser. The heating rate is 10 °C/min, from 30 °C to 1000 °C under the flowing nitrogen environment during this measurement. The UHPC paste is ground to approximately 75 μm after 56 days of curing.

To study the effect of LP on hydration products, the C–S–H contents are calculated. The C–S–H contents can be obtained as follows [36]:

$$\text{C–S–H}(\%) = \frac{M_{\text{CSH}}}{2.1 M_{\text{H}}} \times \Delta m_{\text{CSH}}(\%) \tag{1}$$

where M_{CSH} and M_{H} are the molar masses of C–S–H gel and water, respectively. Δm_{CSH} is the TG mass loss during 150–400 °C.

2.4.3. Mercury intrusion porosimetry

The mercury intrusion porosimetry (MIP) is utilized to measure the pore structure of UHPC pastes after 56 days of curing. About 3.5 g samples are made from the center of the UHPC paste via coring and slicing for measurement. Before the test, the oven is utilized to dry the samples for 48 h at 50 °C.

2.4.4. Nanoindentation test

a) Specimen preparation

After 56 days of curing, the specimens are made into cylinder (diameter: 25 mm, height: 10 mm) from the center of cubic specimens via coring and slicing. The specimen surfaces are initially coarsely grounded by the 400, 800, and 1500 grit polishing papers. Subsequently, a grinding and polishing machine is used for further polishing. Three different diamond suspensions (9 μm, 3 μm, 1 μm) are used in sequential order for finer automatic polishing with matching polishing cloth. Finally, the specimens are washed 5 min with the alcohol solution in an ultrasonic bath.

b) Experimental method

Although the size of the ITZ may differ depending upon the fiber type and fiber size as well as the matrix composition, the majority of previous findings suggested that the thickness of the ITZ ranges from 40 μm to 70 μm [37]. Therefore, nanoindentation grids are performed across the ITZs between the UHPC matrix and the steel fibers. 15 × 10 grids with a grid distance of 5 μm at the horizontal and 10 μm at the vertical directions, as illustrated in Fig. 3. A total of 300 data are obtained from the two randomly selected grids on ITZ of the specimens. The nano-indentation tests are performed using a Hysitron Ti950 Triboindenter and a Berkovich indenter. A trapezoidal loading protocol is utilized in this tests. The load is conducted up to a peak load of 2 mN at the loading rate of 0.2 mN/s, following a holding period of 10 s and an unloading period of 10 s.

The hardness H and elastic modulus E are derived by the Oliver-Pharr method as follows [38]:

$$\text{H} = \frac{P_{max}}{A_c} \tag{2}$$

$$E = (1 - \nu^2)\left(\frac{1}{E_r} - \frac{1 - \nu_i^2}{E_i}\right)^{-1} \tag{3}$$

where P_{max} is the peak load, A_c is the contact area, and ν is the Poisson's ratio of the samples. E_i and ν_i are the elastic modulus and Poisson's ratio of the diamond indenter, respectively. E_r is the reduced modulus, which

Table 2
Mix proportions of UHPC pastes at constant w/p of 0.18, weight %.

Mix	Denote	PC (%)	mS (%)	LP (%)	SP (%)
LP0	PC	100	–	–	1.500
LP10	$PC_{85}mS_5LP_{10}$	85	5	10	1.170
LP20	$PC_{75}mS_5LP_{20}$	75	5	20	1.050
LP30	$PC_{65}mS_5LP_{30}$	65	5	30	0.917
LP40	$PC_{55}mS_5LP_{40}$	55	5	40	0.750
LP50	$PC_{45}mS_5LP_{50}$	45	5	50	0.625

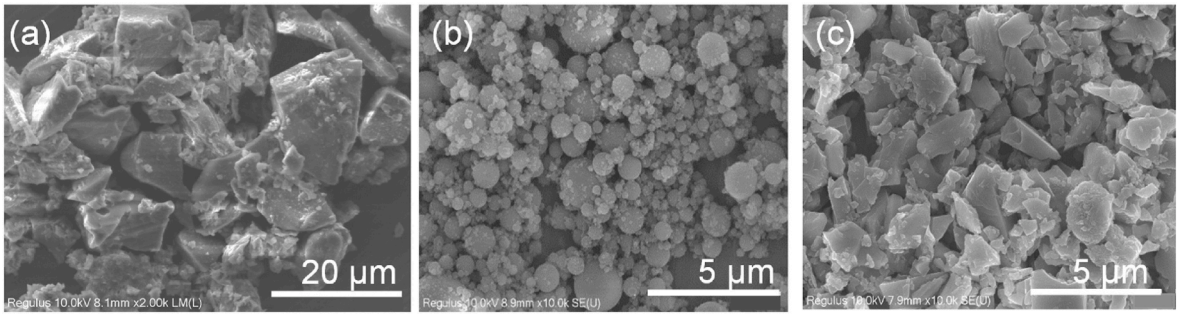

Fig. 2. SEM images of powders: (a) Cement PII · 52.5; (b) Micro-silica (c); Limestone powder.

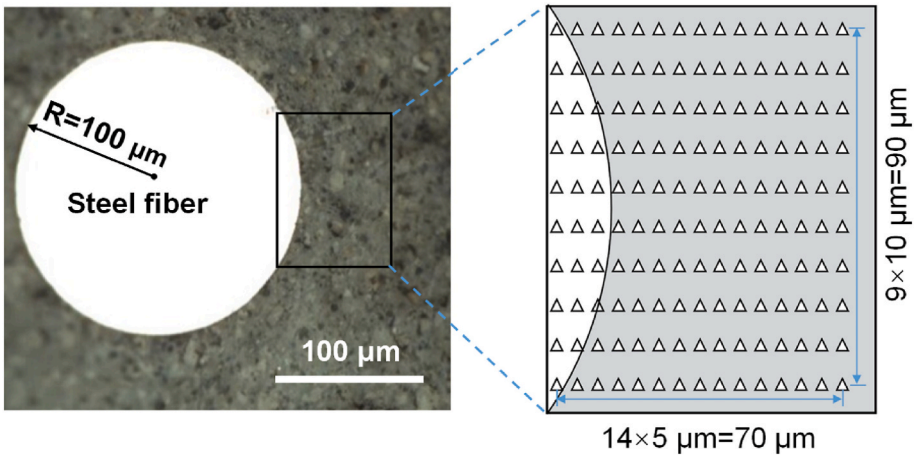

Fig. 3. Schematic of grid indentation for the ITZ of steel fiber.

can be determined by:

$$E_r = \frac{\sqrt{\pi}S}{2\beta\sqrt{A_c}} \tag{4}$$

$$S = \left(\frac{dP}{dh}\right)_{h=h_{max}} \tag{5}$$

where β is a constant depending on the indenter geometry, and S is the contact stiffness.

2.4.5. Quasi-static compressive test

The quasi-static compressive strength is measured by using a compression test apparatus. A invariable loading rate of 1.2 MPa/s is utilized in this test [39]. Three specimens are measured at 28 d and 56 d to determine the mean values of quasi-static compressive strength.

2.4.6. Direct tensile test

Dogbone-shaped specimens are prepared to determine the behavior of UHPC paste with 2% steel fibers under uniaxial tension with displacement rate of 0.1 mm/min. Five specimens are measured for each mixture. The detailed geometrical property of the specimen and the test device are demonstrated in Fig. 4.

2.4.7. Split Hopkinson pressure bar (SHPB) test

The dynamic compressive tests are conducted by utilizing a 50 mm SHPB device, as shown in Fig. 5. The incident pulses (ε_i), reflected (ε_r) and transmitted pulse (ε_t) are measured by strain gauges attached in the center of the incident and transmitted bar. The following assumptions are often made in the dynamic tests: (1) The wave propagation through the bars follows one–dimensional wave theory; (2) The stress and strain states are uniaxial and uniform within the specimen [40]. The stress equilibrium condition and uniform deformation during the dynamic loading are assumed (i.e., $P_1 = P_2, \varepsilon_i(t) + \varepsilon_r(t) = \varepsilon_t(t)$). During the SHPB test, a pulse shaper is adopted to ensure stress equilibrium. Stress $\sigma_s(t)$, strain $\varepsilon_s(t)$ and strain rate $\dot{\varepsilon}_s(t)$ can be obtained, as follows:

$$\sigma_s(t) = \frac{P_1 + P_2}{2A_S} = \frac{E_0 A_0}{2A_S}[\varepsilon_i(t) + \varepsilon_r(t) + \varepsilon_t(t)] \tag{6}$$

$$\varepsilon_s(t) = \frac{C_0}{L_S}\int_0^t [\varepsilon_i(t) - \varepsilon_r(t) - \varepsilon_t(t)]dt \tag{7}$$

$$\dot{\varepsilon}_s(t) = \frac{C_0}{L_S}[\varepsilon_i(t) - \varepsilon_r(t) - \varepsilon_t(t)] \tag{8}$$

where P_1, P_2 represent the dynamic force. $E_0 = 210$ GPa, $C_0 = 5172$ m/s and A_0 are the Young's modulus, wave speed and cross section of the bars, respectively. The cross-sectional area and length of the specimen are represented by A_s and L_s, respectively.

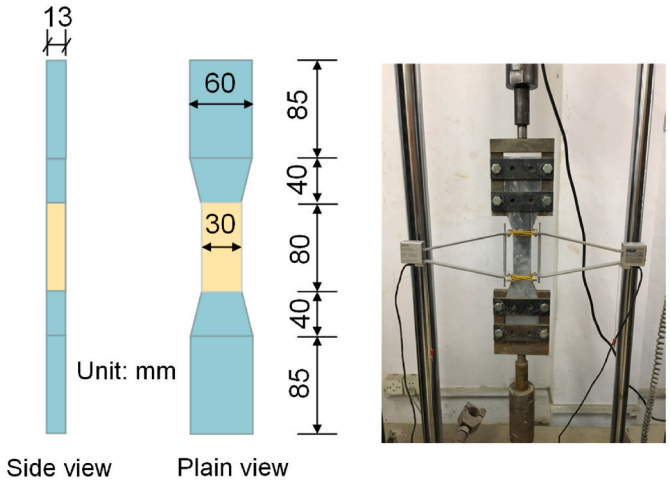

Fig. 4. Dimension of the dog-bone specimen and test device.

3. Results

3.1. Workability

3.1.1. Effect of LP

Sufficient workability of UHPC paste is critical for fiber dispersion and engineering application. The effect of LP replacement on the spread flow of UHPC paste is evaluated. Fig. 6 shows SP dosage required for securing the similar spread flows (270 ± 20) according to the replacement ratios of LP. For LP10~LP50, the SP dosage decreases from 1.17% to 0.625% by mass of powder. It is observed that the flowability of the UHPC pastes is significantly improved when PC is partially replaced by LP, which agrees with the previous conclusion [8,11]. LP has a positive effect on workability owing to its low water demand and electrostatic repulsion effect caused by localizing the Ca^{2+} surface with the groups of OH^- [41]. Additionally, because of its small size and spherical characteristic of mS, water trapped between fine and coarse particles could be displaced by the "ball bearing" effect, improving the workability [42].

3.1.2. Effect of steel fiber

Steel fibers are generally adopted in UHPC, which are distributed

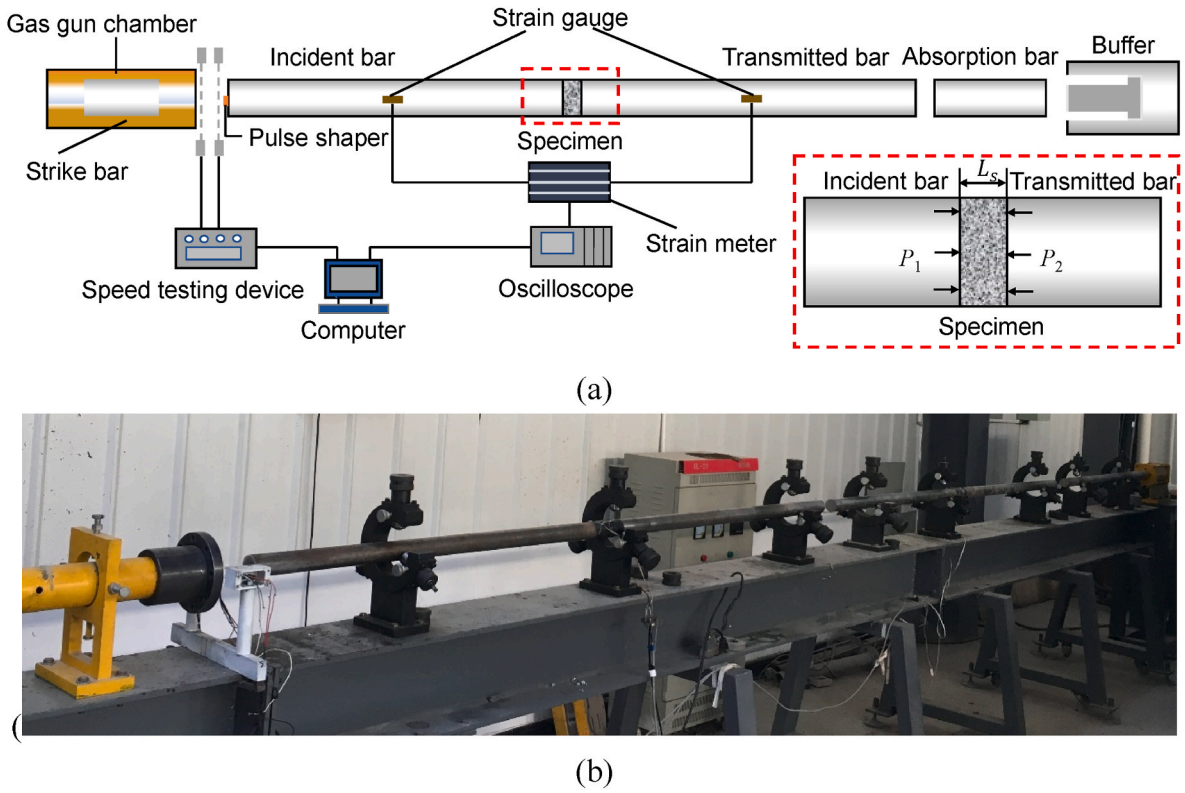

Fig. 5. The SHPB system (a) Schematic diagram; (b) Actual device.

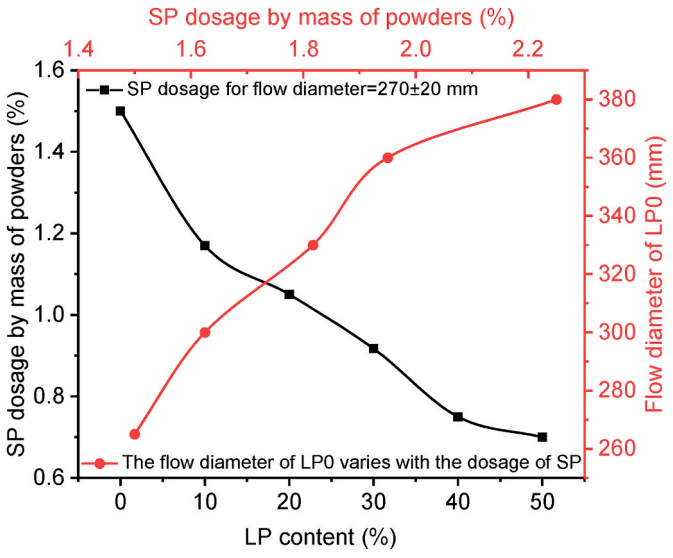

Fig. 6. SP dosage for target flow diameter and the flow diameter of LP0 varies with the dosage of SP.

randomly to transfer the stress within the concrete and inhibit the crack propagation [43]. Non-uniform fiber distribution decreases the strengthening effect of fiber. The flow diameter becomes larger with the increase of SP, as displayed in Fig. 6. For LP0, when the content of SP increases from 1.5% to 2.25%, the flow diameter increases from 265 mm to 385 mm. The flow diameter affects the uniform distribution of steel fiber of the UHPC paste. In this study, the target fluidity of 270 ± 20 mm is achieved by adjusting the SP dosage for the self-consolidating mix. It's noteworthy that the adding steel fibers exhibits rather limited influence on the flow diameter. For example, with the same content of SP, the addition of steel fibers from 1% to 2%, the flow diameter decreases from 273 mm to 265 mm. The small rheological changes of the UHPC agree with the conclusion reported by Martinie et al. [44], who considered that the influence of fibers on the rheological properties is small in the condition that the steel fiber volume fraction is far lower than 3.2/r (r = aspect ratio of steel fiber).

3.2. Hydration products analysis

To study the effect of LP on the hydration products, Fig. 7 presents the TG and DTG results of the UHPC pastes with different LP replacement ratio. Three significant peaks could be found in Fig. 7(b), which are related to the free water loss, dehydration of ettringite, AFm and some calcium silicate hydrate (C–S–H) (30–200 °C); calcium hydroxide (CH) decomposition (400–500 °C); and calcium carbonate ($CaCO_3$) decarbonation (600–800 °C) [10,45]. It can be observed that the third peak becomes stronger and broader with the increase of LP.

To further quantitatively analyze the influence of LP on the hydration product, the C–S–H content by mass of UHPC paste are presented. As shown in Fig. 7(c), the C–S–H content of UHPC rises from 22.5% to 23.5% with the LP substitution increase from 0 to 10%. It may be ascribed to the fact that LP could accelerate the hydration of cement by offering extra surfaces for the nucleation of C–S–H, thereby enhancing the content of C–S–H [46]. More C–S–H generated during the progress of hydration could optimize the microstructure, consequently, improving the mechanical strength of UHPC [29], which will be discussed in Section 3.4. The C–S–H content gradually reduces to 21.6%, 20.3% and 19.4% respectively, with the LP amount increases from 30% to 50%, which could be due to the dilution effect becoming more significant.

3.3. Pore structure analysis

The results of MIP are presented in Fig. 8 to investigate the effect of LP on the pore structures of UHPC paste. The pores size between 8 nm

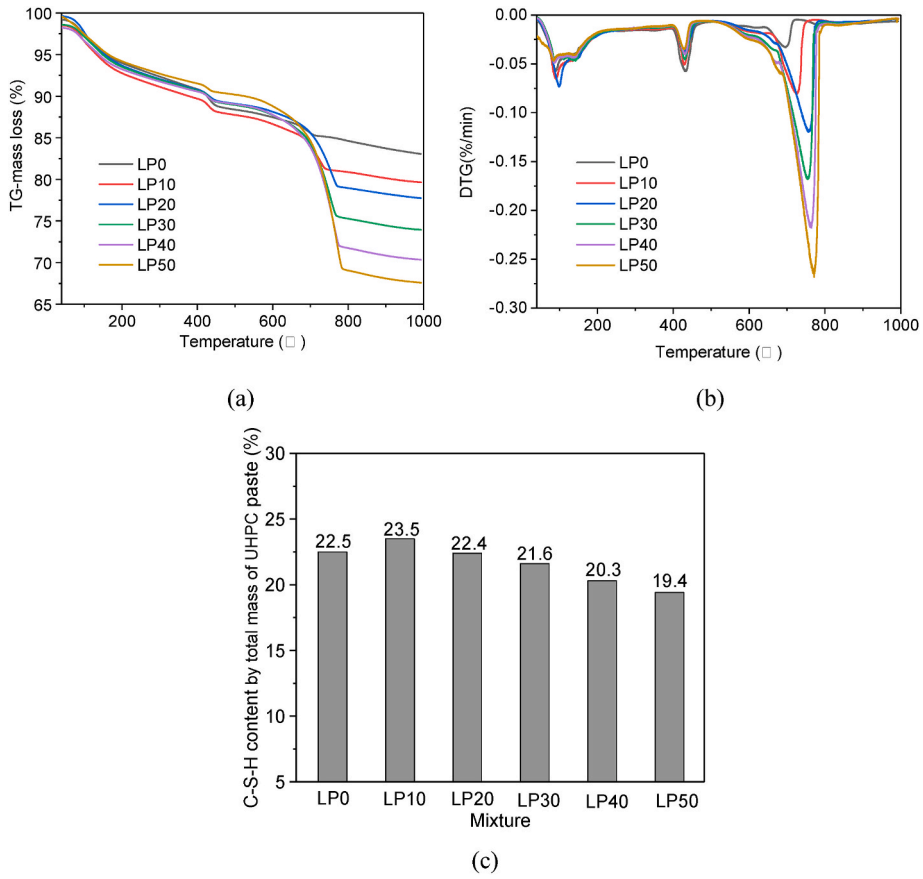

Fig. 7. TG results and C–S–H content of UHPC paste: (a) TG curves; (b) DTG curves; (c) C–S–H content by mass of UHPC paste.

and 50 nm are mainly determined by the content of water and hydration products [47]. As displayed in Fig. 8, compared to LP0, the pore size of LP10 is finer and its capillary pores volume is lower, indicating a denser microstructure. Owing to the pozzolanic effect, the mS reacts with CH, increasing C–S–H volume and decreasing capillary porosity [48]. In addition, excellent filling and nucleation effect of finer LP could refine the pore structure, leading to a more compact microstructure. Nevertheless, with the LP replacement rate increasing from 30% to 50%, the UHPC pastes exhibit much more pores and larger pore size due to the dilution effect.

3.4. Nanoindentation analysis-constituents distribution of ITZ

UHPC matrix is primarily composed of micro-pores (MP), hydration products that contain gel pores in nano size and un-hydrated cement (UC) [49]. As the main hydration products, the C–S–H phases could be divided into low density C–S–H (LD C–S–H) and high density C–S–H (HD C–S–H). Recent studies have revealed that a new phase can be generated under the condition of low w/b, which is expressed as ultra-high density (UHD C–S–H) [31,50]. The elastic modulus of LD C–S–H, HD C–S–H and UHD C–S–H are generally steady despite of different curing methods and w/b. The behavior of these phases can be observed from depth-load curves, as presented in Fig. 9(a).

To quantitatively analyze the hydration products, the experimental data are analyzed using the deconvolution technique [31]. The elastic modulus over 180 GPa are removed to exclude the effects of steel fibers on the hydration products. The test results and theoretical probability density functions (PDF) of the sample (LP50-2) are presented in Fig. 9

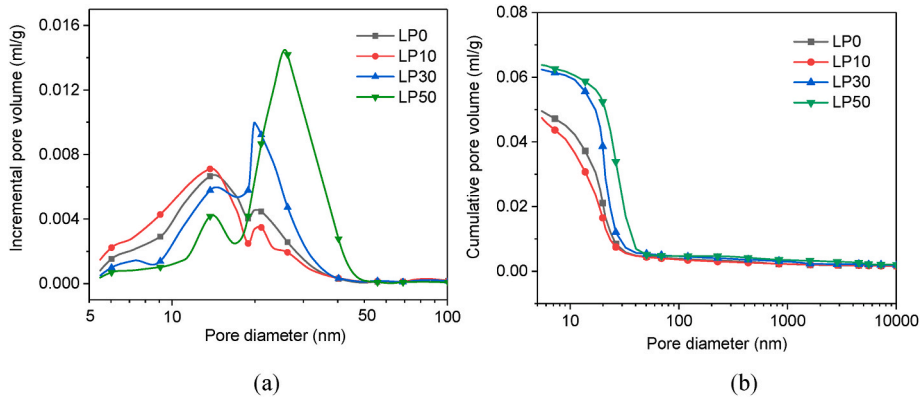

Fig. 8. (a) Pore size distributions; (b) Cumulative pore volume.

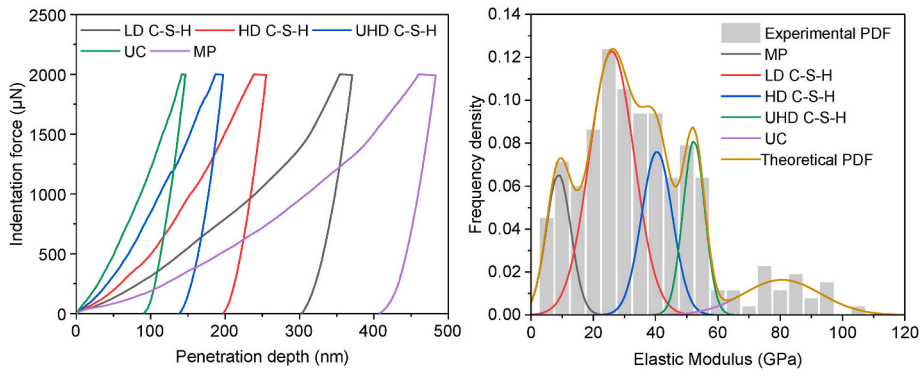

Fig. 9. (a) Typical P-h curves of phases in UHPC matrix; (b) Probability distribution function (PDF) of modulus (LP50-2).

(b). Based on the PDF of the elastic modulus of UHPC, the percentages of each phase in ITZ of UHPC are calculated, as shown in Fig. 10.

Fig. 10(a) presents the effect of LP content on the fractions of MP, C–S–H and UC in ITZ of UHPC. With the LP content increases from 0 to 50%, the percentage of C–S–H improves gradually from 68.3% to 76.1%, while the percentage of UC decreases from 26.4% to 10.3%. It can be concluded that the hydration efficiency of binders in ITZ is enhanced significantly, which is consistent with the results obtained from thermal analysis (see Section 3.2). The MP volume is first reduced to 4.1% at LP10-2 and then slightly increased to 6.5% at LP20-2 and 8.7% at LP30-2, followed by continuous increase from 10.3% to 13.6% at LP40-2 and LP50-2, respectively.

The content of LP not only affects the amount of C–S–H but also has an important effect on its quality. Fig. 10(b) displays the effect of LP content on the percentage of LD C–S–H, HD C–S–H and UHD C–S–H phases in ITZ of UHPC. 10% LP enhances the hydration degree and the content of C–S–H (particularly HD C–S–H and UHD C–S–H) significantly. The percentage of HD C–S–H and UHD C–S–H in LP10-2 increase by 20.2% and 6.8% respectively compared with that of LP0. Nevertheless, the percentage of LD C–S–H in LP10-2 decreases from 6.7% to 4.2%. These results could be interpreted as the fact that nucleation of C–S–H on the LP surface homogenizes the microstructure and facilitates reducing the open capillary porosity [46]. The higher fractions of HD C–S–H and UHD C–S–H would effectively improve the frictional shear stress at the fiber-matrix interface and increase the interfacial bonding strength, thereby improving the mechanical properties of ITZ in UHPC [51]. On the other hand, with the LP content further increasing from 30% to 50%, the percentage of LD C–S–H improves from 20.3% to 35.9%, while the percentage of HD C–S–H and UD C–S–H declines from 36.8% to 25.9% and 17.8%–14.3%, respectively, due to the dilution effect.

3.5. Quasi-static compressive strength

The quasi-static compressive strength at the testing ages of 28 and 56 d are presented in Fig. 11. The 56 days compressive strength of UHPC paste without steel fibers reduces from 150.5 MPa to 99.2 MPa with the LP replacement ratio increasing from 0 to 50%. The 56 days compressive strength exhibits a slight decline from 146.3 MPa at LP10 to 145.2 MPa at LP20, compared to that of LP0. It might be ascribed to the outstanding filling effect and nucleation effect of LP. The mS consumes CH and generates C–S–H gel, improving the compressive strength of UHPC paste. Additionally, an appropriate amount of mS, PC and LP could generate the denser packing to enhance the compressive strength [49]. Therefore, no obvious decrease in strength is observed when the LP replacement rises from 0 to 20%. However, the strengths of UHPC paste tend to decrease significantly when LP replacements more than 30% are used. Due to the dilution effect of excessive LP, the compressive strength of UHPC paste is reduced by 9.4%, 21.7%%, and 34.1% when 30%, 40%, and 50% LP is used compared to that of LP0.

Fig. 11 displays the compressive strength of UHPC paste with steel fiber volumes increasing from 0 to 2%. For a given LP content, the compressive strength gradually rises with the increasing steel fibers, which is consistent with the literature [52]. This could be attributed to the rising of the elastic modulus and good bridging ability of the steel fiber [53]. The 56 days compressive strengths of UHPC with 2% steel fibers range from 113.8 MPa to 178.5 MPa, with the maximum strength at LP10-2. The 56 days compressive strength exhibits a slight rise from 170.6 MPa at LP0-2 to 178.5 MPa at LP10-2. This could be ascribed to

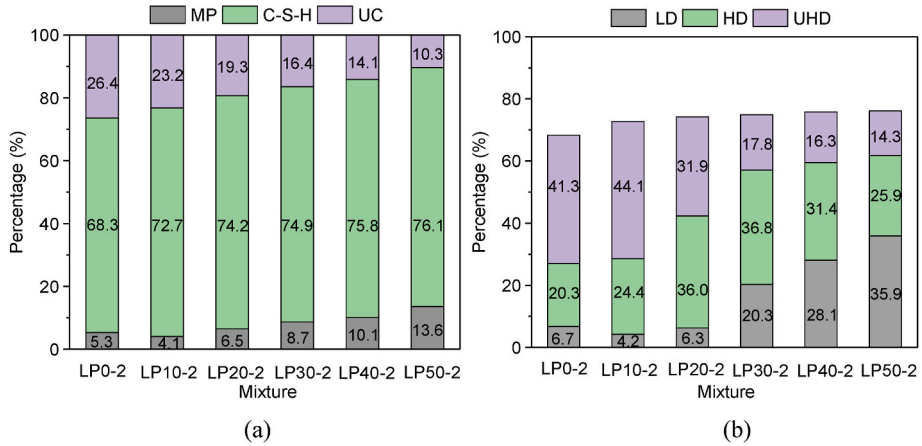

Fig. 10. (a) The percentage of constituent phases in ITZ of UHPC; (b) The percentage of each C–S–H phases in ITZ of UHPC.

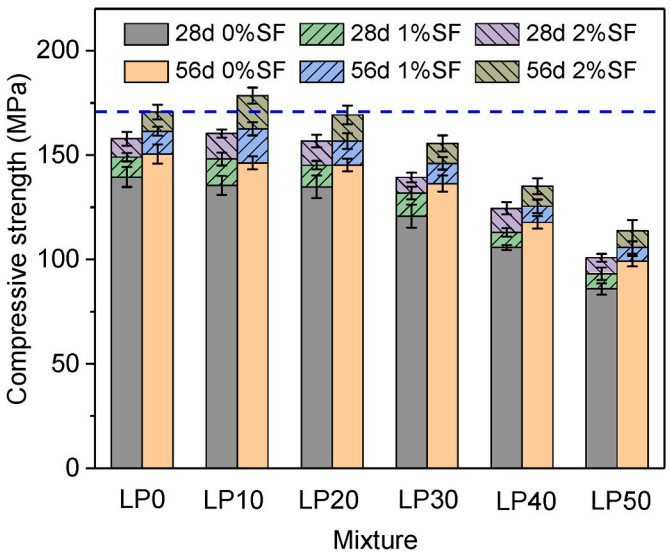

Fig. 11. Quasi-static compressive strength of UHPC paste at the age of 28d and 56d.

the enhanced interfacial bond strength between matrix and steel fiber, which has been discussed in detail in Section 3.4. The 56 days compressive strength of UHPC paste containing 2% steel fibers decreases to 155.6 MPa, 135.1 MPa, 113.8 MPa when 30%, 40%, and 50% LP are introduced, respectively. The sharp decreases could be attributed to the weaker bonding force and less hydration products caused by the dilution effect of excessive LP [8].

3.6. Tensile performance

To analyze the LP content on the tensile performance of UHPC paste containing 2% steel fibers, the measured tensile stress-strain curves are presented in Fig. 12. The specimens show strain hardening behavior with the generation of multiple cracks until the ultimate tensile strength. A slight stress decrease is also observed when new cracks appear, which is similar to the phenomenon previously reported [54–56]. It means that the crack-bridging ability of the steel fibers could effectively be used immediately after the peak point.

The LP10-2 noticeably exhibits the best tensile performance,

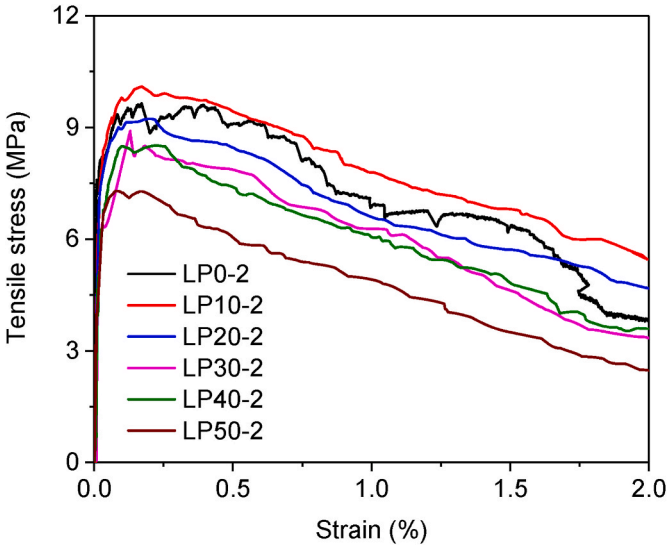

Fig. 12. Effect of LP on tensile stress-strain curve of UHPC paste with 2% steel fibers.

followed by the LP0-2, whereas the LP50-2 exhibits the lowest. The maximum enhancement in the peak tensile strength of LP10-2 is 6.1%, compared to the LP0-2 from 9.53 MPa to 10.11 MPa. The pozzolanic effect of the mS could enhance the fiber-matrix bond strength by replacing CH crystals with C–S–H [8], resulting in enhanced quality in the interface zone. Additionally, the incorporation of LP and mS changes the packing of particles, leading to the denser matrix and higher steel fiber-matrix bond strength, which may compensate for the decline of bond-strength due to the decrease of cement. The further replacement of PC by LP leads to a weaker matrix strength in the interface zone due to the dilution effect, thereby causing the degradation of the reinforcing effect. As the addition of LP increases from 30% to 50%, the peak tensile strength of LP30-2, LP40-2 and LP50-2 gradually decreases by approximately 10.4% to 8.54 MPa, 10.9% to 8.49 MPa, and 23.3% to 7.31 MPa compared to LP0-2, respectively.

3.7. Dynamic compressive properties

3.7.1. Dynamic compressive strength and dynamic increase factor

Fig. 13 presents the variation law of dynamic compressive strength and strain rates of UHPC paste. It can be found that regardless of steel fibers and LP content, the dynamic compressive strength increases with the rising strain rate, exhibiting a significant strain rate effect, which has been widely reported in the previous researches [5,20]. In the case of LP0-2, the peak strength is 162.1 MPa under the strain rate of 93.2 s^{-1}, and increases to 269.55 MPa under the strain rate of 220.1 s^{-1}. The enhancement in the dynamic compressive strength of UHPC paste at a higher strain rate is mainly attributed to the formation of large amount of microcracks, which require a higher energy consumption and lead to higher dynamic compressive strength. Compared with LP0-2, the incorporation of 10% LP and 5% mS of LP10-2 fills the micropores between hydration products and enhances the interface bonding of the UHPC matrix, thereby significantly increasing the energy required for crack formation. Therefore, LP10-2 exhibits the highest dynamic compressive strength (280.25 MPa) among all the tested specimens at the strain rate of 221.5 s^{-1}.

To characterize the strain rate effect, the dynamic increase factor (DIF), which is defined by the ratio of the dynamic compressive strength of the concrete material to its quasi-static compressive strength. The dynamic increase factor (DIF) of UHPC paste containing different steel fibers and LP content under four different strain rates are shown in Fig. 14. It can be found that the values of DIF increase with the strain rate and decrease with the steel fiber content. With the increase of strain rate from 93.2 s^{-1} to 220.1 s^{-1}, the DIF of LP0-2 increases from 0.95 to 1.58 significantly, exhibiting an obvious strain rate effect. For a given LP content, the DIF of UHPC containing 1% steel fibers is higher than that of UHPC paste containing 2% steel fibers, while UHPC with 1% steel fiber is lower than that of UHPC paste, which means that the DIF values of UHPC decrease with the increased content of steel fibers. The reason could be attributed to that steel fibers has an obvious promoting influence on the impact resistance owing to the bridging action of steel fibers, which restrains the propagation of cracks, thereby leading to lower DIFs [57]. The analogous findings were reached by Bischoff and Perry [58], who found that a poorer quality of concrete had a larger DIF. The DIFs of LP0-1, LP0–2, LP10-1, LP10-2, LP20-1, LP20-2 are smaller than 1 at the strain rate of 93.2–98.4 s^{-1}, indicating that the dynamic compressive strength is lower than the quasi-static compressive strength. This might be due to that, at the relative low strain rate (93.2–98.4 s^{-1}), the surface of UHPC specimens is in good condition and not fully damaged (see Fig. 17). Consequently, compared to impact loading, UHPC specimens absorb more energy under quasi-static loading.

For the UHPC with the LP content from 20% to 50%, increasing LP content of UHPC paste typically results in higher DIF of specimens at a given steel fibers content. As illustrated in Fig. 14, UHPC with 50% LP exhibits the highest DIF, followed by that with 40%, 30%, 20% LP at a similar strain rate. However, the DIF values of LP10-1 and LP10-2 are

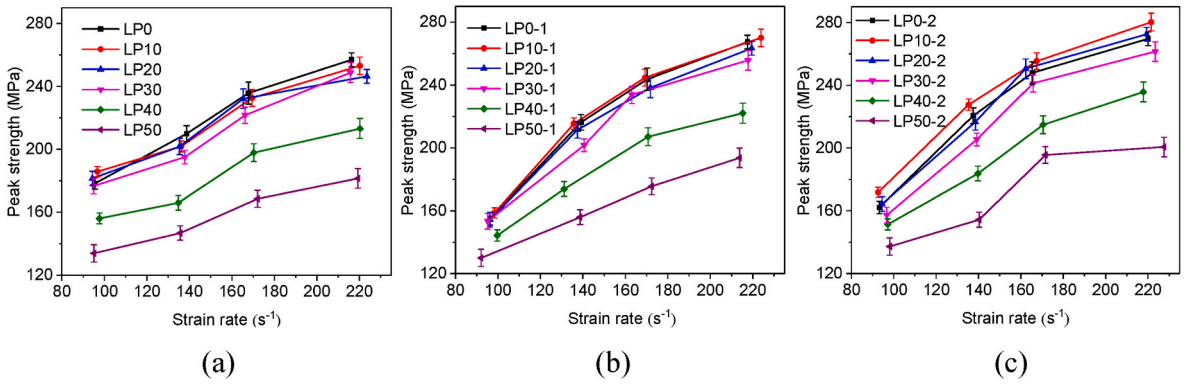

Fig. 13. Relationship between dynamic strength and strain rate: (a) U UHPC paste without steel fibers (b) UHPC paste with 1% steel fibers (c) UHPC paste with 2% steel fibers.

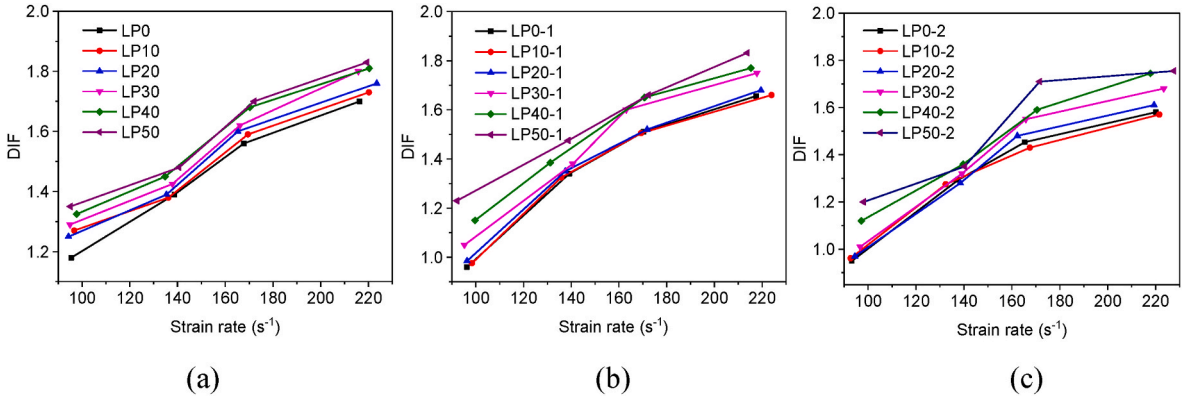

Fig. 14. Relationship between DIF and strain rate: (a) UHPC paste without steel fibers (b) UHPC paste with 1% steel fibers (c) UHPC paste with 2% steel fibers.

lower than that of LP0-1 and LP0-2, respectively. It could ascribe to the better bond property between matrix and steel fibers of LP10-1 and LP10-2, which brings excellent impact resistance.

3.7.2. Stress-strain relationship

The dynamic compressive stress-strain curves of UHPC paste with different steel fibers and LP amount at strain rates of 92.1–227.6 s^{-1} are presented in Fig. 15. Despite the different LP and steel fiber dosage, the shapes of all curves are consistent with each other, which comprises of the rising and descending stages. In the ascending stage, the stress-strain relationship is initially linear elasticity and then exhibits the strain-hardening behavior, where the steel fiber works to restrict the development of micro-cracks [59]. Compared with plain UHPC paste, adding steel fibers enhances the peak strain and ultimate strain of UHPC paste [57]. It could be concluded that the increased steel fibers improve the deformation, which could be interpreted that the crack arresting ability of steel fibers could effectively restrain the propagation speed of cracks in UHPC paste and increase the peak strain. With increased steel fibers, the enclosed area under stress-strain curves increases in the post-peak stage, indicating that adding steel fibers enhances the toughness of UHPC paste [60], leading to a higher energy absorption capacity, which will be discussed in Section 3.7.3.

3.7.3. Energy absorption

The energy absorption is generally expressed as the toughness, which represents the capacity of the UHPC to resist fracture damage under high loading rate [23,61]. The toughness can be obtained based on the stress-strain curve, which is shown as follows [62]:

$$W = \int_0^{\varepsilon} \sigma(\varepsilon) d\varepsilon \tag{9}$$

where W is toughness, σ and ε denote stress and strain, respectively.

The energy absorption of UHPC with different LP and steel fibers contents are presented in Fig. 16. It can be found that the increase of the toughness is proportional to the increasing strain rates and steel fibers for a given LP content. In the case of LP0-2, the energy absorption capacity increases almost 3.67 times from 1.32 MJ/m^3 to 4.84 MJ/m^3 with the strain rate increasing from 93.2 s^{-1} to 220.1 s^{-1}. When the cracks reach the proximity of steel fibers, the stress at crack tips would be transferred to the steel fibers [57]. Then, the stress would be transferred to the surrounding UHPC matrix, resulting in a redistributed stress field. Consequently, the growth of cracks is greatly retarded. When the stress at crack tips surpasses the fiber-matrix bonding force, the steel fibers would be pulled out, along with the amount of energy consumed [63]. More steel fibers are pulled out with the rising strain rate. Thus, more energy is consumed and the impact resistance of UHPC is enhanced. The ultimate strain increases as the amount of steel fiber increases because steel fibers reduce crack formation, which slows down the descending stages of the stress-strain curve [64], demonstrating that adding steel fibers significantly enhances the impact toughness of UHPC. For instance, under the strain rate of 219.3 s^{-1}, the energy absorption ability of LP10-1 and LP10-2 is 4.54 MJ/m^3 and 5.39 MJ/m^3, respectively, which are 23.7% and 46.84% higher than that of LP10. Nevertheless, at the relatively low strain rates (92.1–99.7 s^{-1}), the samples containing steel fibers absorb less energy than that without steel fibers. Samples with steel fibers under lower impact speed are not fractured, leading to the higher reflection and transmission energy, decreasing the absorption

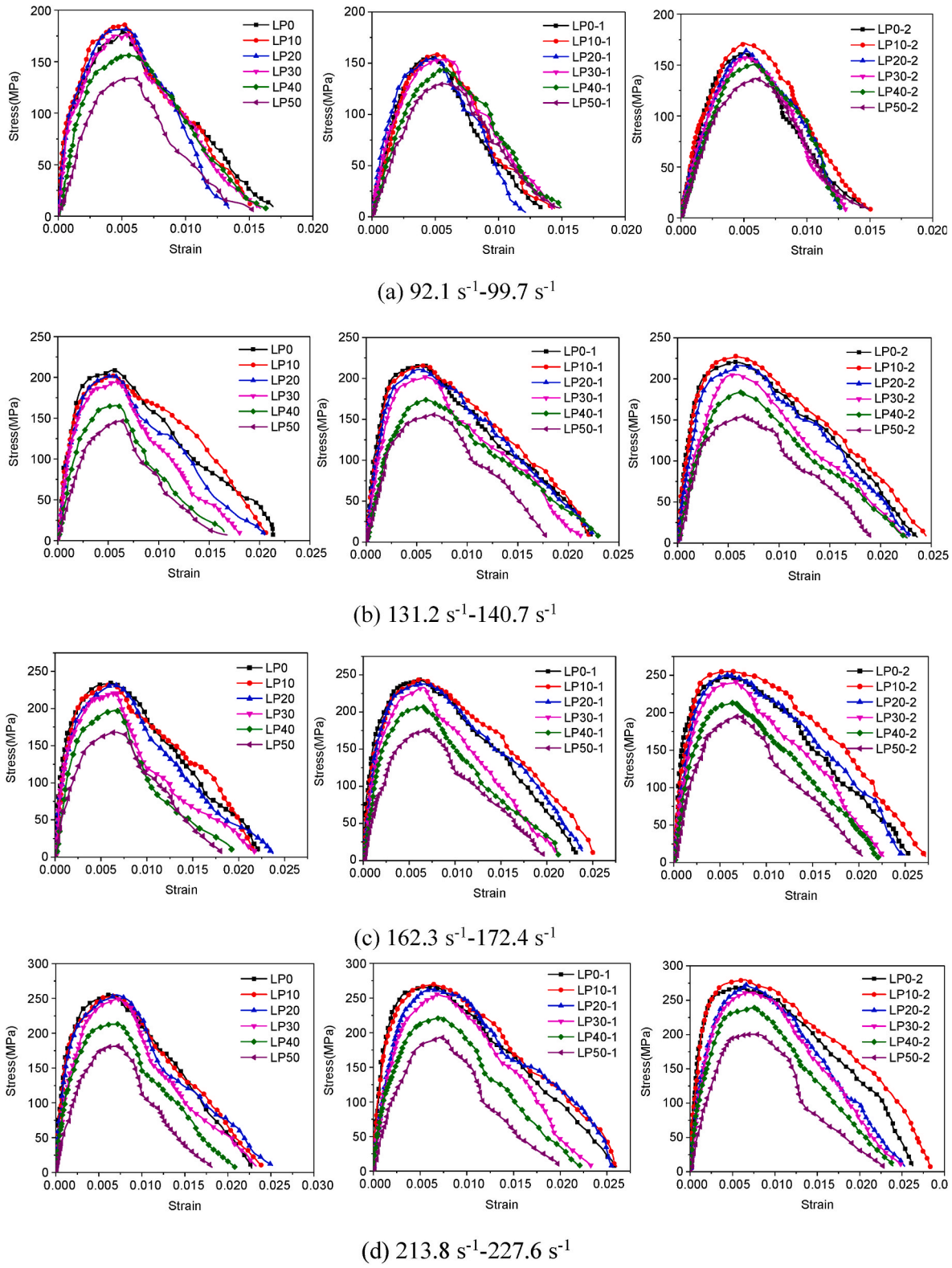

Fig. 15. Dynamic compressive stress-strain curves of UHPC paste under different strain rates.

of energy, the similar finding is reported in literature [65].

It is noteworthy that energy absorption capacity is not only determined by the strength of matrix and steel fiber content, but also affected by the bonding strength between the UHPC matrix and the steel fibers [66]. The energy dissipated by the pullout of steel fibers increases with increasing bonding strength. Therefore, LP10-2 has the highest energy absorption capacity among all mixes because of the excellent bonding strength between the steel fibers and the matrix. With the increase of LP content from 20% to 50%, the energy absorption decreases gradually, which might be explained by the decrease in the strength of the matrix and steel fiber-matrix bond strength due to the dilution effect.

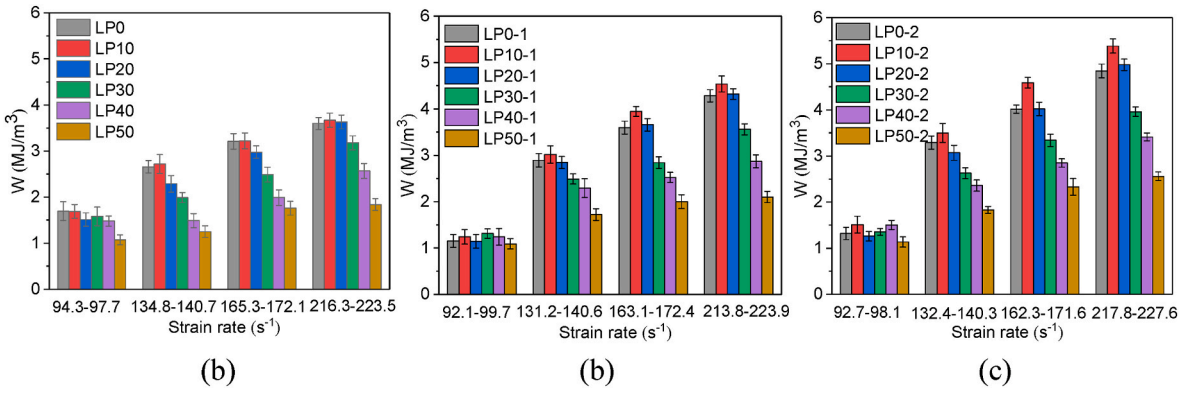

Fig. 16. Relationships between energy absorption and strain rate: (a) UHPC paste without steel fibers (b) UHPC paste with 1% steel fibers (c) UHPC paste with 2% steel fibers.

3.7.4. Failure patterns

The representative dynamic compressive failure patterns of UHPC paste under different strain rates are presented in Fig. 17. The fragmentation degree of UHPC increases significantly with rising of strain rate, and this is consistent with the failure pattern of concrete-like materials under dynamic compressive conditions [20,59,67]. As shown in Fig. 17, at the strain rate of 95.5 s^{-1}, the LP0 breaks into several fragments after failure. With the rising strain rate, the damage degree of specimens becomes more severe. The LP0 is pulverized into numerous small pieces under the strain rate of 167.8 s^{-1}, while the LP0-1 and LP0-2 are still in a split state thanks to the bridging function of steel fibers. Among them, the LP0-2 exhibits the best impact resistance owing to the highest steel fibers content, and only several visible cracks are generated at the strain rate of 97.2 s^{-1}. This phenomenon may be expressed that the pullout of steel fibers can effectively consume a part of the energy during the impact loading, which enhances the energy dissipation capacity of UHPC. In the meantime, increased impact resistance of UHPCs is achieved by the interlaced network structures generated by a large amount of randomly distributed steel fibers that prevents tensile failure caused by crack extension effectively [68].

With the further increase of LP replacement, the bond force between steel fiber and matrix strength is weakened, resulting in a poor bridging effect due to the dilution effect. By analyzing the failure models of UHPC paste with different LP content under similar strain rates, it could be found that the damage degree of LP10-2 is less than other specimens. The reason might be related to that, at the same steel fiber volume fraction, LP10-2 can not only satisfy the amount of effective steel fibers, but also could ensure better steel fiber-matrix bond strength to prevent the specimen from failure. However, more fine-grained pieces are observed with the LP content increasing from 30% to 50% at the same strain rate, implying that the incorporating excess LP reduces the impact resistance of the UHPC paste.

4. Discussions

4.1. Influence of LP on the ITZ of UHPC

The addition of appropriate LP can optimize packing, leading to limited space for the generation of hydration products, where the narrower space could compact new-formed C–S–H densely [69], benefiting the formation of higher quality C–S–H in ITZ. The "wall effect" was proposed by Scrivener et al. [70] to explain the ITZ between the aggregate and concrete mortar. In this study, as steel fiber is 0.2 mm in diameter, which is several to a hundred orders of magnitude larger than cement grains, the steel fiber can be considered as a straight "wall". Therefore, the "wall effect" can also be applied to the fiber-matrix ITZ. According to the "wall effect" [70], finer particles prevail in the vicinity of the wall, while larger particles are found further out, as shown in Fig. 18, given that both the particle sizes of mS and LP are smaller than that of cement. When the cements are replaced by an appropriate replacement of LP, e.g. 10%, the ITZ of UHPC contains the mS and LP predominately, leading to smaller pore size and denser pore structure owing to the excellent filling effect. It has been confirmed that the HD C–S–H and UD C–S–H form in more confined areas because of the limited space [69]. Therefore, more HD C–S–H and UD C–S–H are generated in ITZ of UHPC, leading to an improved transition zone, as shown in Fig. 18(b). This is also demonstrated by the nanoindentation results that the percentage of HD C–S–H and UHD C–S–H increase by 20.2% and 6.8% respectively when cements are replaced with 10% LP and 5% mS. These structural changes of the C–S–H significantly affect the quasi-static mechanical properties of UHPC paste, which are also strong evidences of the interfacial bonding strength change, and they agree with the nanoindentation results. Consequently, the 56 days compressive strength and peak tensile strength of LP10-2 increase by 4.6% and 6.1%, respectively, compared to that of LP0-2.

The addition of LP enhances the effective water-to-cement ratio in the binder system, where usually very low water amount is used, which reduces the content of unhydrated cement, as shown in Fig. 18(b). This phenomenon could be verified by the nanoindentation results, in which the percentage of UC decreases from 26.4% to 10.3% with the LP content increases from 0 to 50%, indicating higher hydration degree of binders. However, while the substitution of cement increases to a high level, the generated C–S–H is not enough to fill the initial space, increasing the pore size and porosity, which is consistent with the MP results. Meanwhile, due to the loose microstructure, the percentage of LD C–S–H and MP of ITZ improves while the percentage of HD C–S–H and UD C–S–H decreases, which deteriorates the strengthening effect of steel fiber. Therefore, the decrease in mechanical properties could be attributed to a rise in porosity and a decrease in HD C–S–H and UHD C–S–H percentage with the increasing LP replacement.

4.2. Influence of LP on the dynamic performance of UHPC

The dynamic compressive performance of UHPC is affected by the matrix and steel fiber. Incorporating an appropriate amount of LP enhances the amount of C–S–H, especially HD C–S–H and UHD C–S–H, and strengthens the ITZ, resulting in a higher steel fiber-matrix bond strength, which can be confirmed by the better strain hardening behavior of UHPC under impact loading (see Section 3.7). A strong interface ensures the efficiency of load transfer between steel fiber and matrix, which would benefit to restricting cracking behavior and improve the dynamic compressive strength and energy absorption capacity [71]. In the case of similar matrix strength, a better bonding ability contributes to more energy consumption by the steel fibers in the process of pulling out, consequently resulting in a better impact resistance.

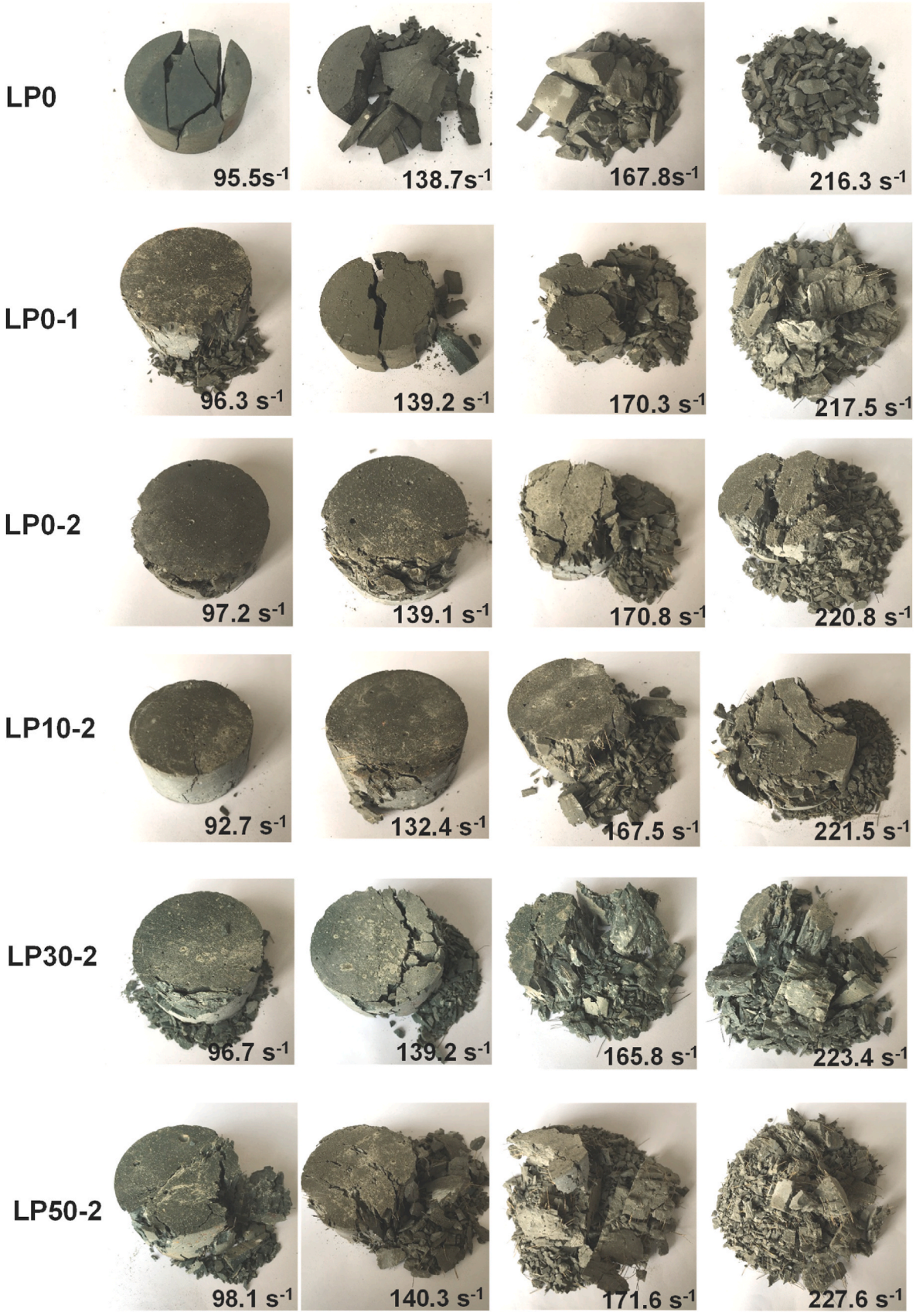

Fig. 17. Failure patterns of UHPC paste under different strain rates.

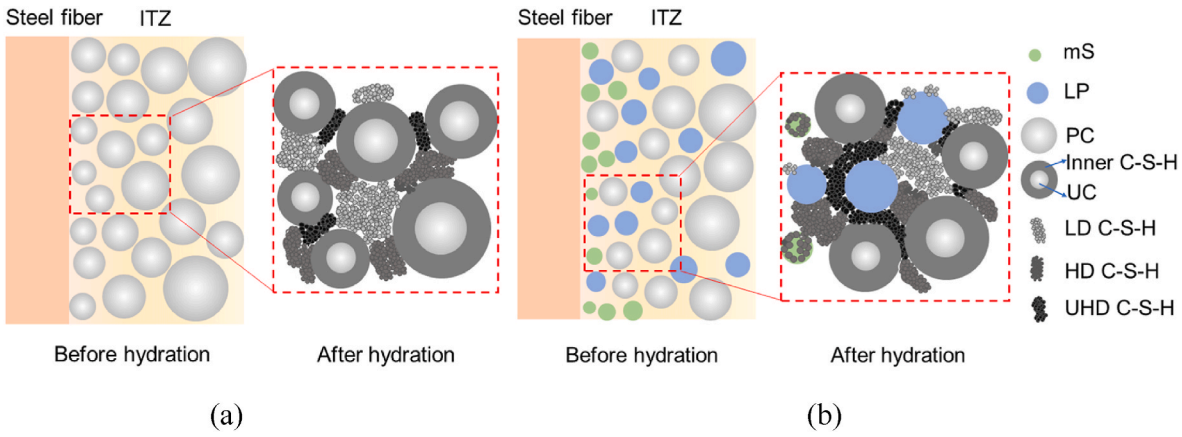

Fig. 18. The enhancement process of ITZ of UHPC induced by LP. (a) 0%LP; (b) 5% mS and 10% LP.

The content of LP leads to different initial micro-cracks, pore structures and interface bonding strength of UHPC paste, which determines the dynamic failure pattern brought by germination and aggregation of micro-cracks [72]. As discussed in Section 3.3, the appropriate substitution of LP, i.e., 10%, can optimize the pore structure, leading to the least pores and micro-cracks. Meanwhile, the steel fiber-matrix interface bonding strength increases owing to the generation of more HD C–S–H and UD C–S–H, resulting in a denser ITZ, which significantly enhances the energy required for the formation of cracks. Steel fibers inhibit the generation of cracks and the higher steel fiber-matrix bond strength leads to the generation of fewer cracks under the same strain rate. Hence, the UHPC paste with 10% LP replacement shows the fewest macro-cracks under the same strain rate, as displayed in Fig. 19(a). The relationship between final failure states of damage and the strain rate is illustrated in Fig. 19(b). The damage state could be divided into split and pulverized, as displayed in Fig. 19(b). Owing to the fewer original defects (e.g., pores, voids and micro-cracks) and denser matrix, as well as a better steel fiber-matrix bond strength, the LP10-2 exhibits the highest strain rates at the split and pulverized states, which means that a higher impact velocity is needed to achieve similar damage, as displayed in Fig. 19(b). The incorporation of excessive LP results in porosity and pore size enlargement as well as more micro-cracks due to the dilution effect, resulting in more macro-cracks generated and more severe damage degree under the same strain rate, which could be confirmed by the failure patterns in Fig. 18. As discussed in Section 3.4, due to lower bond strength caused by excessive LP, the strain rates at the split and pulverized states decrease with the LP content increasing from 30% to 50%, as shown in Fig. 19(b).

5. Conclusions

In this study, the effects of LP on dynamic compressive properties of UHPC are investigated through multi-scale experimental testing and analysis. The hydration products, pore structure, the phase distribution of ITZs and the dynamic compression behaviors of UHPC are analyzed to clarify the relationships between micromechanical properties and macroscopic impact characteristics. The mechanism of LP enhancing the quality and quantity of C–S–H in ITZ between steel fibers and matrix is proposed. The main conclusions can be summarized:

(1) The incorporation of appropriate amount of LP could optimize the packing of particles, resulting in more limited space for the generation of C–S–H that enhances the proportions of HD C–S–H and UHD C–S–H in ITZ. The percentages of HD C–S–H and UHD C–S–H in ITZ increase by 20.2% and 6.8% at replacement of 10% LP, respectively. With the further replacement of LP from 30% to 50%, the volume of LD C–S–H improves while that of UD C–S–H decreases significantly.
(2) The enhanced HD C–S–H and UHD C–S–H contents result in higher fiber-matrix bond strength, which contributes to the quasi-

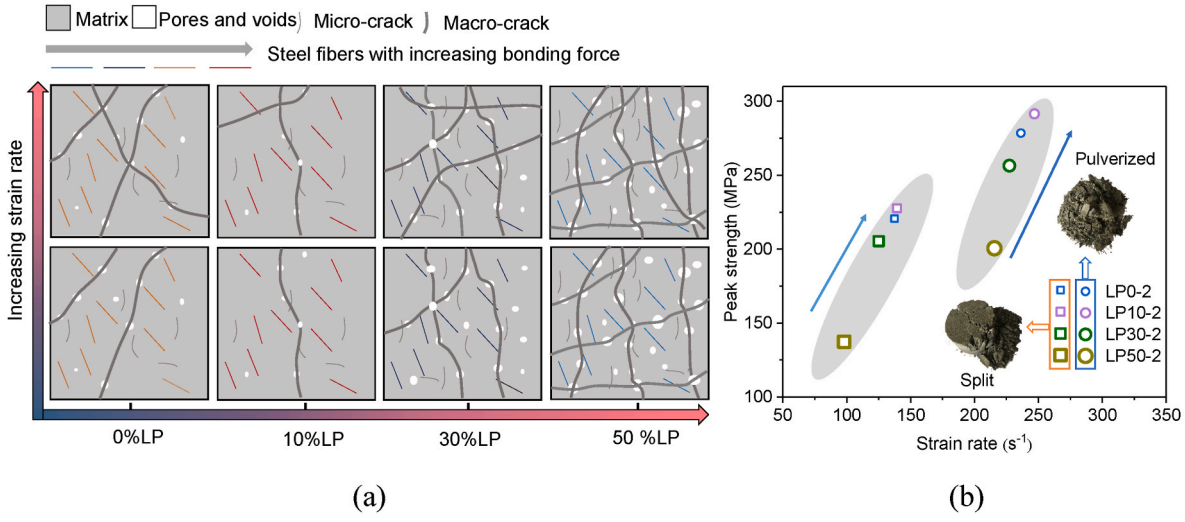

Fig. 19. (a) Schematic diagram of failure patterns of UHPC with different replacement of LP; (b) the relationship between final failure states of damage and strain rate.

static mechanical properties. Therefore, an appropriate substitution of LP, i.e. 10%, contributes to increased quasi-static compressive strength and tensile strength. However, excessive LP content leads to a significant reduction in the quasi-static compressive and tensile strength, attributed to weaker bonding force and less hydration products due to the dilution effect.

(3) The values of DIF increase with the rising strain rate and decrease with the increasing steel fiber content and compactness of microstructure. The appropriate replacement of LP, i.e. 10%, improves bond force between steel fibers and matrix by enhancing the quality of C–S–H, decreasing the porosity and optimizing packing in ITZ. The higher steel fiber-matrix bond strength results in a reduction in the strain rate sensitivity and significantly improves the energy absorption ability of UHPC. With an excessive LP content, the value of DIF increases and energy absorption capacity decreases due to the dilution effect.

(4) A strong interface between the steel fiber and the matrix improves the impact resistance of UHPC. The specimens with appropriate substitution of LP, e.g. 10% exhibit higher strain rates at the split and pulverized states and the lowest degree of damage under a similar strain rate. The strain rates at the split and pulverized states decrease with the LP content, which is mainly attributed to the more generated pores and cracks near the steel fiber-matrix interface, leading to lower bond strength.

CRediT authorship contribution statement

Weitan Zhuang: Methodology, Investigation, Data curation, Formal analysis, Validation, Writing – original draft. **Shaohua Li:** Investigation, Writing – review & editing. **Zhengzhi Wang:** Writing – review & editing. **Zuhua Zhang:** Writing – review & editing. **Qingliang Yu:** Conceptualization, Methodology, Supervision, Funding acquisition, Project administration, Writing – review & editing.

Declaration of competing interest

The authors declare that they have no known competing financial interests or personal relationships that could have appeared to influence the work reported in this paper.

Data availability

Data will be made available on request.

Acknowledgements

This research was carried out under the funding of the National Natural Science Foundation of China (Grant No. 52178246).

References

[1] Shi C, Wu Z, Xiao J, Wang D, Huang Z, Fang Z. A review on ultra high performance concrete: Part I. Raw materials and mixture design. Construct Build Mater 2015; 101:741–51. https://doi.org/10.1016/j.conbuildmat.2015.10.088.

[2] Wang D, Shi C, Wu Z, Xiao J, Huang Z, Fang Z. A review on ultra high performance concrete: Part II. Hydration, microstructure and properties. Construct Build Mater 2015;96:368–77. https://doi.org/10.1016/j.conbuildmat.2015.08.095.

[3] Li PP, Brouwers HJH, Yu Q. Influence of key design parameters of ultra-high performance fibre reinforced concrete on in-service bullet resistance. Int J Impact Eng 2020;136.

[4] Yoo DY, Banthia N. Mechanical and structural behaviors of ultra-high-performance fiber-reinforced concrete subjected to impact and blast. Construct Build Mater 2017;149:416–31.

[5] Yu Q, Zhuang W, Shi C. Research progress on the dynamic compressive properties of ultra-high performance concrete under high strain rates. Cem Concr Compos 2021;124:104258. https://doi.org/10.1016/j.cemconcomp.2021.104258.

[6] Lee J, Lee T, Jeong J, Jeong J. Sustainability and performance assessment of binary blended low-carbon concrete using supplementary cementitious materials. J Clean Prod 2021;280:124373. https://doi.org/10.1016/j.jclepro.2020.124373.

[7] Toledo Filho RD, Koenders EAB, Formagini S, Fairbairn EMR. Performance assessment of ultra high performance fiber reinforced cementitious composites in view of sustainability. Mater Des 2012;36:880–8.

[8] Li PP, Cao YYY, Brouwers HJH, Chen W, Yu QL. Development and properties evaluation of sustainable ultra-high performance pastes with quaternary blends. J Clean Prod 2019;240.

[9] Li PP, Brouwers HJH, Chen W, Yu Q. Optimization and characterization of high-volume limestone powder in sustainable ultra-high performance concrete. Construct Build Mater 2020;242.

[10] Huang W, Kazemi-Kamyab H, Sun W, Scrivener K. Effect of cement substitution by limestone on the hydration and microstructural development of ultra-high performance concrete (UHPC). Cem Concr Compos 2017;77:86–101. https://doi.org/10.1016/j.cemconcomp.2016.12.009.

[11] Bentz DP, Ferraris CF, Jones SZ, Lootens D, Zunino F. Limestone and silica powder replacements for cement: early-age performance. Cem Concr Compos 2017;78: 43–56. https://doi.org/10.1016/j.cemconcomp.2017.01.001.

[12] Kang SH, Jeong Y, Tan KH, Moon J. The use of limestone to replace physical filler of quartz powder in UHPFRC. Cem Concr Compos 2018;94:238–47. https://doi.org/10.1016/j.cemconcomp.2018.09.013.

[13] Moradian M, Hu Q, Aboustait M, Robertson B, Ley MT, Hanan JC, Xiao X. Direct in-situ observation of early age void evolution in sustainable cement paste containing fly ash or limestone. Compos B Eng 2019;175:107099. https://doi.org/10.1016/j.compositesb.2019.107099.

[14] El Fami N, Ez-Zaki H, Boukhari A, Diouri A. Rheological behaviour and mechanical properties of Moroccan ternary binder's Portland clinker-fly ash-limestone. Construct Build Mater 2021;279:122513. https://doi.org/10.1016/j.conbuildmat.2021.122513.

[15] De Weerdt K, Kjellsen KO, Sellevold E, Justnes H. Synergy between fly ash and limestone powder in ternary cements. Cem Concr Compos 2011;33:30–8. https://doi.org/10.1016/j.cemconcomp.2010.09.006.

[16] Burroughs JF, Shannon J, Rushing TS, Yi K, Gutierrez QB, Harrelson DW. Potential of finely ground limestone powder to benefit ultra-high performance concrete mixtures. Construct Build Mater 2017;141:335–42. https://doi.org/10.1016/j.conbuildmat.2017.02.073.

[17] Lothenbach B, Le Saout G, Gallucci E, Scrivener K. Influence of limestone on the hydration of Portland cements. Cement Concr Res 2008;38:848–60.

[18] Ramezanianpour AM, Hooton RD. A study on hydration, compressive strength, and porosity of Portland-limestone cement mixes containing SCMs. Cem Concr Compos 2014;51:1–13. https://doi.org/10.1016/j.cemconcomp.2014.03.006.

[19] Khosravani MR, Weinberg K. A review on split Hopkinson bar experiments on the dynamic characterisation of concrete. Construct Build Mater 2018;190:1264–83.

[20] Zhuang W, Li S, Yu Q. The effect of supplementary cementitious material systems on dynamic compressive properties of ultra-high performance concrete paste. Construct Build Mater 2022;321:126361. https://linkinghub.elsevier.com/retrieve/pii/S0950061822000551.

[21] Ragalwar K, Heard WF, Williams BA, Kumar D, Ranade R. On enhancing the mechanical behavior of ultra-high performance concrete through multi-scale fiber reinforcement. Cem Concr Compos 2020;105:103422. https://doi.org/10.1016/j.cemconcomp.2019.103422.

[22] Teng L, Meng W, Khayat KH. Rheology control of ultra-high-performance concrete made with different fiber contents. Cement Concr Res 2020;138:106222. https://doi.org/10.1016/j.cemconres.2020.106222.

[23] Zhang B, Feng Y, Xie J, He J, Zhang Y, Cai C, Huang D, Li L. Effects of fibres on ultra-lightweight high strength concrete: dynamic behaviour and microstructures. Cem Concr Compos 2022;128:104417. https://doi.org/10.1016/j.cemconcomp.2022.104417.

[24] Shi C, Wang D, Wu L, Wu Z. The hydration and microstructure of ultra high-strength concrete with cement-silica fume-slag binder. Cem Concr Compos 2015; 61:44–52. https://doi.org/10.1016/j.cemconcomp.2015.04.013.

[25] Faheem A, Rizwan SA, Bier TA. Properties of self-compacting mortars using blends of limestone powder, fly ash, and zeolite powder. Construct Build Mater 2021;286: 122788. https://doi.org/10.1016/j.conbuildmat.2021.122788.

[26] Li Y, Kwan AKH. Ternary blending of cement with fly ash microsphere and condensed silica fume to improve the performance of mortar. Cem Concr Compos 2014;49:26–35.

[27] min Zhan P, hai He Z, ming Ma Z, feng Liang C, xiang Zhang X, Abreham AA, yan Shi J. Utilization of nano-metakaolin in concrete: a review. J Build Eng 2020;30: 101259. https://doi.org/10.1016/j.jobe.2020.101259.

[28] Gautham S, Sasmal S. Recent Advances in Evaluation of intrinsic mechanical properties of cementitious composites using nanoindentation technique. Construct Build Mater 2019;223:883–97. https://doi.org/10.1016/j.conbuildmat.2019.07.002.

[29] Li S, Jensen OM, Wang Z, Yu Q. Influence of micromechanical property on the rate-dependent flexural strength of ultra-high performance concrete containing coarse aggregates (UHPC-CA). Compos B Eng 2021;227. https://doi.org/10.1016/j.compositesb.2021.109394. 109394.

[30] Konstantopoulos G, Koumoulos E, Karatza A, Charitidis C. Pore and phase identification through nanoindentation mapping and micro-computed tomography in nanoenhanced cement. Cem Concr Compos 2020;114:103741. https://doi.org/10.1016/j.cemconcomp.2020.103741.

[31] Xu L, Deng F, Chi Y. Nano-mechanical behavior of the interfacial transition zone between steel-polypropylene fiber and cement paste. Construct Build Mater 2017; 145:619–38. https://doi.org/10.1016/j.conbuildmat.2017.04.035.

[32] Xu J, Corr DJ, Shah SP. Nanomechanical investigation of the effects of nanoSiO2 on C-S-H gel/cement grain interfaces. Cem Concr Compos 2015;61:7–17. https://doi.org/10.1016/j.cemconcomp.2015.04.011.

[33] Li PP, Yu QL, Brouwers HJH. Effect of coarse basalt aggregates on the properties of Ultra-high Performance Concrete (UHPC). Construct Build Mater 2018;170:649–59.
[34] Wang L, Yang L, Dong X, Jiang X. Dynamic experimental study on the distortional law of materials. 2019.
[35] EN-1015-3. Methods of test for mortar for masonry – Part 3:Determination of consistence of fresh mortar (by flow table). Br. Stand. Institution-BSI CEN Eur. Comm. Stand. 2007.
[36] Jain J, Neithalath N. Analysis of calcium leaching behavior of plain and modified cement pastes in pure water. Cem Concr Compos 2009;31:176–85. https://doi.org/10.1016/j.cemconcomp.2009.01.003.
[37] Wang XH, Jacobsen S, He JY, Zhang ZL, Lee SF, Lein HL. Application of nanoindentation testing to study of the interfacial transition zone in steel fiber reinforced mortar. Cement Concr Res 2009;39:701–15. https://doi.org/10.1016/j.cemconres.2009.05.002.
[38] Oliver WC, Pharr GM. An improved technique for determining hardness and elastic madulus using load and displacement. J Mater Res 1992;7:1564–83.
[39] GB/T 50081-2002. Standard test methods for mechanical properties of ordinary concrete[S]. 2015.
[40] Z. X. Z. L.L. Wang, Basic of stress wave, 1985.
[41] Li PP, Yu QL. Responses and post-impact properties of ultra-high performance fibre reinforced concrete under pendulum impact. Compos Struct 2019;208:806–15.
[42] Wu Z, Khayat KH, Shi C. Changes in rheology and mechanical properties of ultra-high performance concrete with silica fume content. Cement Concr Res 2019;123:105786. https://doi.org/10.1016/j.cemconres.2019.105786.
[43] Koutný O, Snoeck D, Van Der Vurst F, De Belie N. Rheological behaviour of ultra-high performance cementitious composites containing high amounts of silica fume. Cem Concr Compos 2018;88:29–40.
[44] Martinie L, Rossi P, Roussel N. Rheology of fi ber reinforced cementitious materials : classi fi cation and prediction. Cement Concr Res 2010;40:226–34. https://doi.org/10.1016/j.cemconres.2009.08.032.
[45] Wu Z, Shi C, Khayat KH. Influence of silica fume content on microstructure development and bond to steel fiber in ultra-high strength cement-based materials (UHSC). Cem Concr Compos 2016;71:97–109. https://doi.org/10.1016/j.cemconcomp.2016.05.005.
[46] Dhandapani Y, Santhanam M, Kaladharan G, Ramanathan S. Towards ternary binders involving limestone additions — a review. Cement Concr Res 2021;143:106396. https://doi.org/10.1016/j.cemconres.2021.106396.
[47] De Belie N, Kratky J, Van Vlierberghe S. Influence of pozzolans and slag on the microstructure of partially carbonated cement paste by means of water vapour and nitrogen sorption experiments and BET calculations. Cement Concr Res 2010;40:1723–33. https://doi.org/10.1016/j.cemconres.2010.08.014.
[48] Dale PES, Bentz P. Evolution of porosity and calcium hydroxide in laboratory concretes containing silica fum. Cement Concr Res 1994;24:1044–50.
[49] hai He Z, gui Du S, Chen D. Microstructure of ultra high performance concrete containing lithium slag. J Hazard Mater 2018;353:35–43. https://doi.org/10.1016/j.jhazmat.2018.03.063.
[50] Vandamme M, Ulm FJ, Fonollosa P. Nanogranular packing of C-S-H at substochiometric conditions. Cement Concr Res 2010;40:14–26. https://doi.org/10.1016/j.cemconres.2009.09.017.
[51] Sharma R, Jang JG, Bansal PP. A comprehensive review on effects of mineral admixtures and fibers on engineering properties of ultra-high-performance concrete. J Build Eng 2022;45:103314. https://doi.org/10.1016/j.jobe.2021.103314.
[52] Song Q, Yu R, Shui Z, Rao S, Wang X, Sun M, Jiang C. Steel fibre content and interconnection induced electrochemical corrosion of Ultra-High Performance Fibre Reinforced Concrete (UHPFRC). Cem Concr Compos 2018;94:191–200. https://doi.org/10.1016/j.cemconcomp.2018.09.010.
[53] Ren GM, Wu H, Fang Q, Liu JZ. Effects of steel fiber content and type on static mechanical properties of. UHPCC 2018;163:826–39.
[54] Kim J, Jang YS, Yoo D. Enhancing the tensile performance of ultra-high-performance concrete through novel curvilinear steel fibers. Integr. Med. Res. 2020;9:7570–82. https://doi.org/10.1016/j.jmrt.2020.05.072.
[55] Oh T, You I, Banthia N, Yoo DY. Deposition of nanosilica particles on fiber surface for improving interfacial bond and tensile performances of ultra-high-performance fiber-reinforced concrete. Compos B Eng 2021;221:109030. https://doi.org/10.1016/j.compositesb.2021.109030.
[56] Yoo D, Shin W, Chun B. Corrosion effect on tensile behavior of ultra-high-performance concrete reinforced with straight steel fibers. Cem Concr Compos 2020;109:103566. https://doi.org/10.1016/j.cemconcomp.2020.103566.
[57] Li N. Impact resistance of steel fiber-reinforced self-compacting concrete (SCC) at high strain rates. 2021. p. 38.
[58] Bischoff SHPPH. Compressive behaviour of concrete at high strain rates. Mater Struct 1991;24:425–50.
[59] Ren GM, Wu H, Fang Q, Liu JZ. Effects of steel fiber content and type on dynamic compressive mechanical properties of UHPCC. Construct Build Mater 2018;164:29–43.
[60] Lai D, Demartino C, Xiao Y. High-strain rate compressive behavior of fiber-reinforced rubberized concrete. Construct Build Mater 2022;319:125739. https://doi.org/10.1016/j.conbuildmat.2021.125739.
[61] Tang Z, Li W, Tam VWY, Luo Z. Investigation on dynamic mechanical properties of fly ash/slag-based geopolymeric recycled aggregate concrete. Compos B Eng 2020;185:107776. https://doi.org/10.1016/j.compositesb.2020.107776.
[62] Miyoshi MIT, Mukai T. Enhancement of energy absorption in a closed-cell aluminum by the modification of cellular structures. Scripta Mater 1999;41(10):1055–60.
[63] Wang J, Dong S, Dai Pang S, Yu X, Han B, Ou J. Tailoring anti-impact properties of ultra-high performance concrete by incorporating functionalized carbon nanotubes. Engineering 2021. https://doi.org/10.1016/j.eng.2021.04.030.
[64] Kseniia R, Zhou W. Dynamic compressive response of high-performance fiber-reinforced cement composites. Construct Build Mater 2020;249:118738. https://doi.org/10.1016/j.conbuildmat.2020.118738.
[65] Tai YS. Uniaxial compression tests at various loading rates for reactive powder concrete. Theor Appl Fract Mech 2009;52:14–21.
[66] Fu Q, Bu M, Xu W, Chen L, Li D, He J, Kou H, Li H. Comparative analysis of dynamic constitutive response of hybrid fibre-reinforced concrete with different matrix strengths. Int J Impact Eng 2020;148:103763.
[67] Wei H, Zhou A, Liu T, Zou D, Jian H. Dynamic and environmental performance of eco-friendly ultra-high performance concrete containing waste cathode ray tube glass as a substitution of river sand. Resour Conserv Recycl 2020;162:105021. https://doi.org/10.1016/j.resconrec.2020.105021.
[68] Jiang J, Feng T, Chu H, Wu Y, Wang F, Zhou W, Wang Z. Quasi-static and dynamic mechanical properties of eco-friendly ultra-high-performance concrete containing aeolian sand. Cem Concr Compos 2019;97:369–78.
[69] Liu Y, Zhuge Y, Chow CWK, Keegan A, Ma J, Hall C, Li D, Pham PN, Huang J, Duan W, Wang L. Cementitious composites containing alum sludge ash: an investigation of microstructural features by an advanced nanoindentation technology. Construct Build Mater 2021;299:124286. https://doi.org/10.1016/j.conbuildmat.2021.124286.
[70] Scrivener KL, Crumbie AK, Laugesen P. The interfacial transition zone (ITZ) between cement paste and aggregate in concrete. Interface Sci 2004;12:411–21.
[71] Yao X, Shamsaei E, Wang W, Zhang S, Sagoe-crentsil K. Graphene-based modi fi cation on the interface in fi bre reinforced cementitious composites for improving both strength and toughness. Carbon N. Y. 2020;170:493–502. https://doi.org/10.1016/j.carbon.2020.08.051.
[72] Yao W, Xu Y, Xia K. Damage evolution during rock pulverization induced by dynamic compressive loading. J Geophys Res Solid Earth 2020;125:1–22.